EurJIC European Journal of Inorganic Chemistry

FULL PAPER

DOI: 10.1002/ejic.201200228

Synthesis and Characterization of a (μ-η²:η²-Peroxido)dicopper(II) Complex with *N*,*N*′,*N*′′-Triisopropyl-*cis*,*cis*-1,3,5-triaminocyclohexane (R_3TACH, R = *i*Pr): Selective Preparation of (μ-η²:η²-Peroxido)dicopper(II) and Bis(μ-oxido)-dicopper(III) Species Regulated by Substituent Groups

Jun Matsumoto,[a] Yuji Kajita,[a] and Hideki Masuda*[a]

Keywords: Bioinorganic chemistry / Copper / Coordination modes / Hydroxylation

The new Cu^{I} complex of *N*,*N*′,*N*′′-triisopropyl-*cis*,*cis*-1,3,5-triaminocyclohexane (*i*Pr_3TACH), [Cu(*i*Pr_3TACH)(MeCN)](X), immediately reacts with dioxygen at –80 °C to give a (μ-η²:η²-peroxido)dicopper(II) complex. This observation is significantly different from the previously reported cases of bis(μ-oxido)dicopper(III) complexes that were generated by the reaction of copper(I) complexes of other TACH ligands (Et_3TACH, *i*Bu_3TACH, and Bn_3TACH) with dioxygen under the same reaction conditions. Such selective preparations have been explained in terms of the structural specificity provided by the TACH ligands that surround the metal centers. The obtained (μ-η²:η²-peroxido)dicopper(II) complex exhibits *ortho*-hydroxylation of a phenolate to *ortho*-quinone with ca. 50 % yield based on the peroxido intermediate. The bis(μ-oxido)dicopper(III) complexes with other TACH derivatives are not capable of oxygenation of phenolate. The (μ-η²:η²-peroxido)dicopper core is discussed in the context of the reaction mechanism of tyrosinase.

Introduction

The bioinorganic chemistry of copper has inspired the development of synthetic systems as models to help us understand the functions of metalloproteins.[1–13] Type 3 copper centers, which are found in the active sites of copper metalloproteins such as hemocyanin (Hc), tyrosinase (Ty), and catechol oxidase (CaO), play an important role in binding and/or activating dioxygen at their dimetallic sites.[14–16] These proteins contain a dinuclear copper core with six coordinated histidine imidazole groups and participate in various biologically essential functions. For example, Hc serves as a dioxygen carrier,[17] Ty catalyzes the *ortho*-hydroxylation of phenols to *ortho*-quinones,[8] and CaO catalyzes the oxidation of *ortho*-catechols to *ortho*-quinones.[16] Ty not only catalyzes the *ortho*-hydroxylation of phenols, but it also catalyzes reversible oxygenation reactions similar to Hc[18] and the oxidation of phenols to catechols similar to CaO.[19,20] In the reaction of oxytyrosinase (oxyTy) with a phenolate substrate, the most interesting step in the monophenolase cycle of Ty is the insertion of an oxygen atom at the *ortho* position of the phenol C–OH group by oxyTy. Model studies using low molecular weight metal complexes can be very helpful in elucidating reaction mechanisms and identifying reaction intermediates. To elucidate the structure–function relationships of these enzymes, various bioinorganic studies have been reported.

In 1989, Kitajima et al. provided the first report of a complex with a (μ-η²:η²-peroxido)dicopper(II) structure [Cu^{II}_2-(μ-η²:η²-peroxido)($Tp^{iPr,iPr}$)$_2$, $Tp^{iPr,iPr}$ = hydrotris-(3,5-diisopropylpyrazolyl)borato],[21] which was proposed as a structural model of the oxyHc active site. The oxyHc active site structure was confirmed by X-ray crystallography in 1994.[22,23] Subsequently, Tolman et al. identified another interesting bis(μ-oxido)dicopper(III) species and demonstrated that it is reversibly converted into the (μ-η²:η²-peroxido)dicopper(II) species.[24–26] We also previously prepared these two species using sparteine as a ligand, which are controlled by carboxylate coordination.[27] Based on these two intermediate species, the mechanism of tyrosinase activity has been discussed by several groups.

Casella et al. and Itoh et al. have reported that the Ty activity of the (μ-η²:η²-peroxido)dicopper(II) species depends upon the coordination of a phenolate anion to the metal center. However, these reports did not provide any direct evidence.[28–34] On the other hand, Stack et al. prepared a [Cu^{II}_2(μ-η²:η²-peroxido)(DBED)$_2$]$^{2+}$ complex using a bidentate DBED ligand (DBED = *N*,*N*′-di-*tert*-butylethylenediamine), and found that it is converted to a bis(μ-oxido)dicopper(III) species, [Cu^{III}_2(μ-O)$_2$(phenolate)-(DBED)$_2$]$^{2+}$, upon axial coordination of the phenolate substrate to the metal ion to give *ortho*-catechol and *ortho*-quinone.[35,36] It was claimed that the coordination of the phenolic oxygen atom to the metal atom promotes the for-

[a] Department of Frontier Materials, Graduate School of Engineering, Nagoya Institute of Technology
Showa-ku, Nagoya 466-8555, Japan
Fax: +81-52-735-5228
E-mail: masuda.hideki@nitech.ac.jp

Supporting information for this article is available on the WWW under http://dx.doi.org/10.1002/ejic.201200228.

mation of bis(μ-oxido)dicopper(III) species from (μ-η^2:η^2-peroxido)dicopper(II) species, and that the active intermediate of Ty is the bis(μ-oxido)dicopper(III) species. Costas et al. have also shown that the bis(μ-oxido)dicopper(III) cores induce *ortho*-hydroxylation of phenolate anions using the dinuclear dicopper complex with a dinucleating ligand, which has three or four coordination sites.[37] Furthermore, it was reported that a *trans*-μ-η^1:η^1-peroxidodicopper(II) complex with an unsymmetrical heptadentate ligand is also capable of *ortho*-hydroxylation of phenolate.[38,39] On the other hand, Casella et al. demonstrated in spectroscopic studies using native Ty that the active species of Ty is the (μ-η^2:η^2-peroxido)dicopper(II) species and that the *ortho*-hydroxylation of phenol proceeds through coordination of phenol to the copper atom.[40] Tuczek and Casella et al. described *ortho*-hydroxylation using a model system comprised of a dinuclear copper complex with α,α′-bis[bis{2-(1′-methyl-2′-benzimidazolyl)ethyl}amino]-*m*-xylene,[30] and recently Tuczek et al. succeeded in observing catalytic hydroxylation of a coordinated phenolate anion using a mononuclear copper(I) complex with a bidentate ligand 2,2-dimethyl-1-[2-(pyrid-2-yl)ethyl]iminopropane, phenolate, and triethylamine.[41] The actual reaction mechanism of Ty has not yet been confirmed.

We previously synthesized copper(I) complexes of *N*,*N*′,*N*′′-trialkyl-*cis*,*cis*-1,3,5-triaminocyclohexane derivatives (R_3TACH), which have ethyl (Et_3TACH), isobutyl (iBu$_3$TACH), or benzyl groups (Bn_3TACH) at the secondary amine nitrogen atoms, as Hc and/or Ty active center models, and studied their reactions with dioxygen to produce the corresponding bis(μ-oxido)dicopper(III) complexes. The reaction intermediates are capable of oxidizing THF as an exogenous substrate to give 2-hydroxytetrahydrofuran and γ-butyrolactone, but they do not oxidize phenol.[42,43] At this stage, we synthesized a new triaminocyclohexane derivative ligand, *N*,*N*′,*N*′′-triisopropyl-*cis*,*cis*-1,3,5-triaminocyclohexane (iPr$_3$TACH), in which the α-carbon atom is a tertiary one. This is slightly different from the previously designed R_3TACH ligands, which have a secondary carbon atom. The R_3TACH ligands may be slightly flexible in coordinating the metal atom, whereas iPr$_3$TACH is expected to be less flexible and to form a tight structure for coordinating the metal ion as shown in Figure S1. Additionally, as speculated from the crystal structures of bis(μ-hydroxido)dicopper(II) complexes with R_3TACH (R = Et, *i*Bu, or Bn), the substituent groups can easily rotate around the N–C_R bond because of the intramolecular steric hindrance between two ligands[43] as compared with the isopropyl group in iPr$_3$TACH. Interestingly, the copper(I) complex with iPr$_3$TACH immediately reacts with dioxygen to form only the (μ-η^2:η^2-peroxido)dicopper(II) complex. This is in contrast to the previously reported copper(I) complexes with other R_3TACH ligands that only form bis(μ-oxido)dicopper(III) species. Here we have succeeded in the selective preparation of (μ-η^2:η^2-peroxido)dicopper(II) and bis(μ-oxido)dicopper(III) cores using copper complexes with R_3TACH derivative ligands. In this paper, we describe the preparation and characterization of these complexes using electronic absorption, electrochemical, IR, and X-ray analytical methods, and also discuss the oxidation reactivity of the (μ-η^2:η^2-peroxido)dicopper(II) complex with respect to phenolate.

Results and Discussion

Synthesis and Characterization of Copper(I) Complexes

The copper(I) complexes with the iPr$_3$TACH ligand, [Cu(MeCN)(iPr$_3$TACH)]X [**1**$^{i\mathrm{Pr}}$(MeCN)·X, X = SbF_6 or OTf], were synthesized by the reactions of [Cu(MeCN)$_4$]X (X = SbF_6 or OTf) with iPr$_3$TACH in tetrahydrofuran (THF) under anaerobic conditions. The formulations for the complexes were determined by ^{1}H NMR spectroscopy, IR spectroscopy, mass spectrometry, and elemental analysis. **1**$^{i\mathrm{Pr}}$(MeCN)·SbF_6 and **1**$^{i\mathrm{Pr}}$(MeCN)·OTf were recrystallized from THF/Et_2O. The coordination of MeCN to the copper(I) ions in **1**$^{i\mathrm{Pr}}$(MeCN)·SbF_6 and **1**$^{i\mathrm{Pr}}$(MeCN)·OTf was confirmed by the observation of IR bands assigned to ν(C≡N) at 2264 and 2265 cm^{-1}, respectively, which lie in the range of those of the previously reported copper(I) complexes with other TACH ligands and an MeCN molecule; 2280 cm^{-1} for Et_3TACH, 2250 cm^{-1} for iBu$_3$TACH, and 2270 cm^{-1} for Bn_3TACH. The carbonylcopper(I) complexes with iPr$_3$TACH, [Cu(CO)(iPr$_3$TACH)]OTf [**1**$^{i\mathrm{Pr}}$(CO)·OTf] and [Cu(CO)(iBu$_3$TACH)]PF_6 [**1**$^{i\mathrm{Bu}}$(CO)·PF_6], were prepared by treating complexes **1**$^{i\mathrm{Pr}}$(MeCN)·OTf and **1**$^{i\mathrm{Bu}}$(MeCN)·PF_6 with CO in CH_2Cl_2 at 0 °C. Single crystals of **1**$^{i\mathrm{Pr}}$(CO)·OTf and **1**$^{i\mathrm{Bu}}$(CO)·PF_6 suitable for X-ray analysis were obtained by recrystallization from CH_2Cl_2/Et_2O under Ar. IR spectra for **1**$^{i\mathrm{Pr}}$(CO)·OTf and **1**$^{i\mathrm{Bu}}$(CO)·PF_6 have absorption bands assignable to ν(C≡O) at 2058 and 2068 cm^{-1}, respectively. These values are in the range of previously reported carbonylcopper(I) complexes with other TACH derivative ligands (Bn_3TACH, iBu$_3$TACH, and Et_3TACH) and *N*,*N*′,*N*′′-triisopropyl-1,4,7-triazacyclononane (iPr$_3$TACN), and N,*N*′,*N*′′-triisopropyl-1,5,9-triazacycldodecane (iPr$_3$TACD);[43,44] 2055 cm^{-1} for Et_3TACH, 2057 cm^{-1} for iBu$_3$TACH, 2076 cm^{-1} for Bn_3TACH, 2063 cm^{-1} for iPr$_3$TACD, and 2067 cm^{-1} for iPr$_3$TACN. These results are indicative of carbonylcopper(I) complexes with tetrahedral geometry.

Crystal Structures of Copper(I) Complexes

The structure of **1**$^{i\mathrm{Pr}}$(MeCN)·SbF_6 was determined by X-ray crystallography. The crystallographic data are listed in Table 8. The structure of the cationic part of **1**$^{i\mathrm{Pr}}$(MeCN)·SbF_6 and selected bond lengths and angles are shown in Figure 1 and Table 1, respectively.

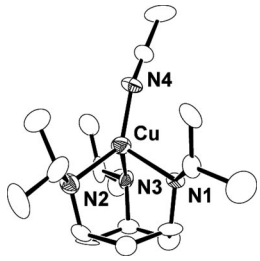

Figure 1. ORTEP view of the cationic portions of $\mathbf{1}^{i\mathrm{Pr}}$(MeCN)·$SbF_6$ with the atom numbering scheme (30% probability ellipsoids).

Table 1. Selected bond lengths [Å] and angles [°] for $\mathbf{1}^{i\mathrm{Pr}}$(MeCN)·$SbF_6$.

Cu–N(1)	2.114(6)	N(1)–Cu–N(4)	113.8(2)
Cu–N(2)	2.049(6)	N(2)–Cu–N(4)	135.9(2)
Cu–N(3)	2.114(6)	N(1)–Cu–N(2)	96.8(2)
Cu–N(4)	1.875(6)	N(1)–Cu–N(3)	94.9(2)
		N(2)–Cu–N(3)	96.5(2)
		N(3)–Cu–N(4)	110.9(2)

The molecular structure of the cationic part of $\mathbf{1}^{i\mathrm{Pr}}$(MeCN)·$SbF_6$ has tetrahedral geometry with three secondary amine nitrogen atoms of the $i\mathrm{Pr}_3$TACN ligand and an MeCN molecule coordinated to the metal ion. The average Cu–N_{TACH} bond, 2.092(6) Å, is slightly shorter than those of the copper(I) complexes with other TACH ligands reported previously; Cu–N_{TACH} 2.108(5) Å for Et_3TACH, 2.120(2) Å for $i\mathrm{Bu}_3$TACH, and 2.1318(6) Å for Bn_3TACH.[43] These results may suggest that the ability of $i\mathrm{Pr}_3$TACH to donate electrons to the metal ion is greater than the electron-donor capability of Et_3TACH, $i\mathrm{Bu}_3$-TACH, and Bn_3TACH. However, the coordinated MeCN molecule is affected by the supporting ligands, and the Cu–N_{MeCN} bond of $\mathbf{1}^{i\mathrm{Pr}}$(MeCN)·$SbF_6$, 1.875(6) Å, tends to become shorter than those of copper(I) complexes with other TACH ligands [Cu–N_{MeCN} 1.881(5) Å for Et_3TACH, 1.900(2) Å for $i\mathrm{Bu}_3$TACH, and 1.880(2) Å for Bn_3TACH]. In general, stronger electron donation from the supporting ligands to the copper(I) ions makes the binding of MeCN weaker based on consideration of Pauling's neutralization theory.[45] The results obtained here are the opposite. Although we do not have specific evidence to explain this phenomenon, it is possible that the copper ion is repulsively compressed by the *i*Pr methyl groups as seen in the space-filling model in Figure S1.

Tolman et al. have reported on the relationship between the structures and oxygenation reactivities of copper(I) complexes with $i\mathrm{Pr}_3$TACN and $i\mathrm{Pr}_3$TACD ligands.[44] It was concluded that the dioxygen reactivity is significantly affected by the magnitude of the deviations of the Cu ion from the mean plane defined by the three N-donor atoms (the N_3 plane) and the mean plane defined by the three *i*Pr methine carbon atoms [the $(CH)_3$ plane] for the macrocyclic ligands.[44] Copper complexes with smaller macrocyclic ligands exhibit higher oxygenation reactivities relative to those of copper complexes with larger ligands. It is unclear if this also applies to the current complex. The deviations of the copper(I) ions from the N_3 plane and the $(CH)_3$ plane in the *N*-alkyl substituent groups for $\mathbf{1}^{i\mathrm{Pr}}$(MeCN)·$SbF_6$ are 1.0724(16) and 0.6860(16) Å, respectively (Table 2 and Figure 2). Interestingly, these values are significantly smaller than those of copper(I) complexes with other TACH derivative ligands; 1.1046(6) and 0.7177(6) Å for Et_3TACH, 1.1161(3) and 0.7713(3) Å for $i\mathrm{Bu}_3$TACH, 1.1187(17) and 0.7079(17) Å for Bn_3TACH. This indicates that the metal ion of $\mathbf{1}^{i\mathrm{Pr}}$(MeCN)·$SbF_6$ is compressed relative to the metal ion in $\mathbf{1}^{\mathrm{Et}}$(MeCN)·SbF_6, $\mathbf{1}^{i\mathrm{Bu}}$(MeCN)·$SbF_6$, and $\mathbf{1}^{\mathrm{Bn}}$-(MeCN)·SbF_6. As described in the electrochemistry section below, $\mathbf{1}^{i\mathrm{Pr}}$(MeCN)·$SbF_6$ has a higher redox potential than the other copper(I) complexes with R_3TACH (R = Et, *i*Bu, and Bn). The higher potential may be related to this structural feature.

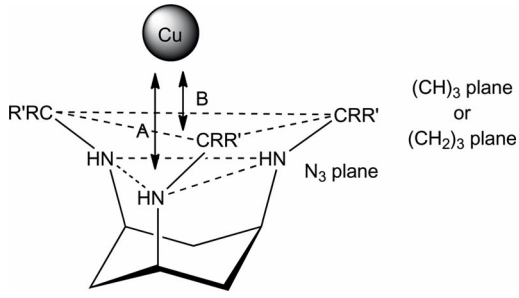

Figure 2. Deviation of copper ions from the N_3 plane defined by three amine nitrogen atoms (A) and the $(CH_x)_3$ plane defined by three methylene or methine carbon atoms (B).

The carbonylcopper(I) adduct, $\mathbf{1}^{i\mathrm{Pr}}$(CO)·OTf, was recrystallized from CH_2Cl_2/Et_2O to produce a single crystal suitable for X-ray structure analysis. For comparison, we also synthesized $\mathbf{1}^{i\mathrm{Bu}}$(CO)·$PF_6$ and characterized it by X-ray structure analysis. Crystal data and relevant experimental details are summarized in Table 8. Molecular structures and

Table 2. FTIR spectroscopic data [cm^{-1}] and deviations of copper ions from the planes defined by three amine nitrogen atoms and three α-carbon atoms [Å].

Complex	*v*(N≡C)	Cu···N_3	Cu···$(CH)_3$/Cu···$(CH_2)_3$	Ref.
$\mathbf{1}^{i\mathrm{Pr}}$(MeCN)·$SbF_6$	2264	1.0724(16)	0.6860(16)	this work
$\mathbf{1}^{\mathrm{Et}}$(MeCN)·SbF_6	2280	1.1046(6)	0.7177(6)	[43]
$\mathbf{1}^{i\mathrm{Bu}}$(MeCN)·$SbF_6$	2250	1.1161(3)	0.7713(3)	[43]
$\mathbf{1}^{\mathrm{Bn}}$(MeCN)·SbF_6	2270	1.1187(17)	0.7079(17)	[43]
[Cu(MeCN)($i\mathrm{Pr}_3$TACN)]BPh_4	–	1.40	0.70	[44]
[Cu(MeCN)($i\mathrm{Pr}_3$TACD)]SbF_6	–	1.26	–0.02	[44]

selected bond lengths and angles for $\mathbf{1}^{i\mathrm{Pr}}$(CO)·OTf and $\mathbf{1}^{i\mathrm{Bu}}$(CO)·$PF_6$ are given in Figures 3 and 4, and Tables 3 and 4, respectively.

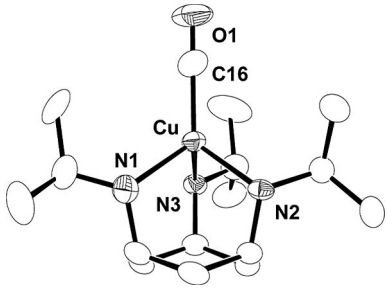

Figure 3. ORTEP view of the cationic portions of $\mathbf{1}^{i\mathrm{Pr}}$(CO)·OTf with the atom numbering scheme (30% probability ellipsoids).

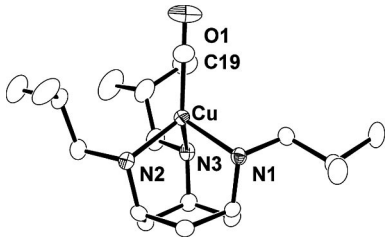

Figure 4. ORTEP view of the cation of $\mathbf{1}^{i\mathrm{Bu}}$(CO)·$PF_6$ with the atom numbering scheme (30% probability ellipsoids).

Table 3. Selected bond lengths [Å] and angles [°] for $\mathbf{1}^{i\mathrm{Pr}}$(CO)·OTf.

Cu–C(16)	1.808(4)	N(1)–Cu–N(2)	94.40(12)
Cu–N(1)	2.092(3)	N(1)–Cu–N(3)	97.06(12)
Cu–N(2)	2.093(2)	N(2)–Cu–N(3)	96.29(10)
Cu–N(3)	2.080(3)	C(16)–Cu–N(1)	118.40(16)
		C(16)–Cu–N(2)	120.03(16)
		C(16)–Cu–N(3)	124.24(17)

Table 4. Selected bond lengths [Å] and angles [°] for $\mathbf{1}^{i\mathrm{Bu}}$(CO)·$PF_6$.

Cu–C(19)	1.800(2)	N(1)–Cu–N(2)	95.73(5)
Cu–N(1)	2.0967(14)	N(1)–Cu–N(3)	95.51(5)
Cu–N(2)	2.0631(15)	N(2)–Cu–N(3)	95.07(5)
Cu–N(3)	2.1025(12)	C(19)–Cu–N(1)	114.03(9)
		C(19)–Cu–N(2)	122.37(8)
		C(19)–Cu–N(3)	127.12(7)

Both $\mathbf{1}^{i\mathrm{Pr}}$(CO)·OTf and $\mathbf{1}^{i\mathrm{Bu}}$(CO)·$PF_6$ have tetrahedral coordination geometry with the copper atoms bonded to three amine nitrogen atoms of the TACH ligand and a carbon monoxide ligand. The Cu–C and C≡O bond lengths of $\mathbf{1}^{i\mathrm{Pr}}$(CO)·OTf and $\mathbf{1}^{i\mathrm{Bu}}$(CO)·$PF_6$ are 1.808(4)/1.103(5) and 1.800(2)/1.110(3) Å, respectively. The Cu–C and C≡O bond lengths of the previously reported carbonylcopper(I) complex with Bn_3TACH, $\mathbf{1}^{\mathrm{Bn}}$(CO)·SbF_6, in which the crystal contains two independent molecules in the unit cell, were 1.813(5)/1.129(7) and 1.777(6)/1.152(7) Å, respectively. The stronger coordination of the carbonyl ligand to the metal atom appears to have weakened the C≡O bonds. The Cu–C and C≡O bonds of $\mathbf{1}^{i\mathrm{Pr}}$(CO)·OTf tend to be slightly longer and shorter, respectively, than those of the other two complexes. These findings indicate that the electron-donating capability of $i\mathrm{Pr}_3$TACH is slightly weaker than those of the $i\mathrm{Bu}_3$TACH and Bn_3TACH ligands. The average Cu–N_{TACH} bonds of $\mathbf{1}^{i\mathrm{Pr}}$(CO)·OTf and $\mathbf{1}^{i\mathrm{Bu}}$(CO)·$PF_6$, 2.088(3) and 2.087(2) Å, respectively, are slightly longer than those of the carbonylcopper(I) complexes with Bn_3TACH [2.058(8), 2.060(7) Å]. These tendencies do not correlate with the results from the crystal structures of the acetonitrile complexes. The Cu–N_{TACH} bonds for the carbonyl complexes are all shorter than those of the corresponding acetonitrile complexes; this is considered to have been caused by a decrease in the electron density of the copper(I) ion by backdonation to the carbonyl ligand. From these results, the effect of the steric hindrance of the substituents does not significantly affect these carbonylcopper(I) systems. In terms of the displacement of the metal ion from the N_3 and $(CH)_3$ planes, the same tendency observed for (acetonitrile)copper(I) systems was also identified in the carbonylcopper(I) systems; however, these differences are less than those in the (acetonitrile)copper(I) systems. The Cu···N_3 and Cu···$(CH)_3$ distances for $\mathbf{1}^{i\mathrm{Pr}}$(CO)·OTf are 1.0739(5)/0.6664(5) Å. These distances are shorter than those of $\mathbf{1}^{i\mathrm{Bu}}$(CO)·$PF_6$ and $\mathbf{1}^{\mathrm{Bn}}$(CO)·SbF_6, 1.0849(3)/0.6867(3), and 1.0805(7)/0.6961(7) and 1.1209(7)/0.7501(7) Å, respectively (Table 5). This result is also justified above.

Electrochemical Properties

In order to study the reactivity of $\mathbf{1}^{i\mathrm{Pr}}$(MeCN)·$SbF_6$ with dioxygen and its reversible oxygenation activity, the redox potential of $\mathbf{1}^{i\mathrm{Pr}}$(MeCN)·$SbF_6$ was measured by cyclic voltammetry in a CH_2Cl_2/MeCN (9:1, v/v) mixed solution (Figure S2 and Table 6).

Table 5. FTIR spectral data [cm^{-1}] and deviations of the copper ions from the planes defined by three amine nitrogen atoms and three α-carbon atoms [Å].

Complex	ν(C≡O)	Cu···N_3	Cu···$(CH)_3$/Cu···$(CH_2)_3$	Ref.
$\mathbf{1}^{i\mathrm{Pr}}$(CO)·OTf	2058	1.0739(5)	0.6664(5)	this work
$\mathbf{1}^{\mathrm{Et}}$(CO)·SbF_6	2055	–	–	[43]
$\mathbf{1}^{i\mathrm{Bu}}$(CO)·$SbF_6$	2057	–	–	[43]
$\mathbf{1}^{i\mathrm{Bu}}$(CO)·$PF_6$	2068	1.0849(3)	0.6867(3)	this work
$\mathbf{1}^{\mathrm{Bn}}$(CO)·SbF_6	2076	1.1209(7)	0.7501(7)	[43]
		1.0805(7)	0.6961(7)	[43]
[Cu(MeCN)($i\mathrm{Pr}_3$TACN)]BPh_4	2063	–	–	[44]
[Cu(MeCN)($i\mathrm{Pr}_3$TACD)]SbF_6	2067	–	–	[44]

Table 6. Electrochemical properties [mV] for copper(I) complexes.

Complex	$E_{1/2}$[b]	ΔE_p[b]	E_{pa}[b]	E_{pc}[b]	Ref.
$\mathbf{1}^{i\mathrm{Pr}}$(MeCN)·$SbF_6$[a]	447	99	496	397	this work
$\mathbf{1}^{\mathrm{Et}}$(MeCN)·SbF_6	344	109	398	289	[43]
$\mathbf{1}^{i\mathrm{Bu}}$(MeCN)·$SbF_6$	394	113	450	337	[43]
$\mathbf{1}^{\mathrm{Bn}}$(MeCN)·SbF_6	346	105	398	293	[43]
[Cu(MeCN)(*i*Pr$_3$TACN)]BPh_4	570	510			[44]
[Cu(MeCN)(*i*Pr$_3$TACD)]SbF_6	600	180			[44]

[a] Potentials were measured in a CH_2Cl_2/MeCN (9:1, v/v) mixed solution with the supporting electrolyte 0.1 M nBu$_4$NClO_4 (TBAP). The working, counter, and reference electrodes used were GC, Pt, and Ag/Ag$^+$(MeCN), respectively. The scan rate is 50 mV/s. [b] Reported vs. SCE.

A quasireversible wave was observed with an $E_{1/2}$ value of 447 mV vs. SCE and an ΔE_p value of 99 mV. The $E_{1/2}$ value of $\mathbf{1}^{i\mathrm{Pr}}$(MeCN)·$SbF_6$ is significantly higher than those of $\mathbf{1}^{\mathrm{Et}}$(MeCN)·SbF_6 (344 mV), $\mathbf{1}^{i\mathrm{Bu}}$(MeCN)·$SbF_6$ (394 mV), and $\mathbf{1}^{\mathrm{Bn}}$(MeCN)·SbF_6 (346 mV) in spite of the fact that the TACH derivatives all have a secondary amine. This is very similar to the case of copper complexes with TACN and TACD derivative ligands; the redox potentials of the copper complexes with the *i*Pr group are observed in the positive region relative to those of their corresponding copper(I) complexes with methyl and benzyl groups. The electrochemical study indicated that the *i*Pr$_3$TACH stabilizes the lower oxidation states, but the crystal structure of $\mathbf{1}^{i\mathrm{Pr}}$(MeCN)·$SbF_6$ suggested that the donation ability of *i*Pr$_3$TACH ligand is stronger than the others. In order to elucidate the contradictory findings, we carefully examined the angles around the Cu–N bond. We found an interesting value in the C_R–N–C_{TACH} angle. The C_R–N–C_{TACH} bond angle of $\mathbf{1}^{i\mathrm{Pr}}$(MeCN)·$SbF_6$ [av. 114.0(6)°] is slightly larger than the corresponding angles for $\mathbf{1}^{\mathrm{Et}}$(MeCN)·SbF_6 [av. 112.6(4)°], $\mathbf{1}^{i\mathrm{Bu}}$(MeCN)·$SbF_6$ [av. 111.9(2)°], and $\mathbf{1}^{\mathrm{Bn}}$(MeCN)·SbF_6 [av. 112.2(4)°]. Although all of these angles are significantly larger than the 109.28° angle of an idealized sp^3-hybridized orbital, the corresponding angle of $\mathbf{1}^{i\mathrm{Pr}}$(MeCN)·$SbF_6$ is especially large. This larger bond angle for $\mathbf{1}^{i\mathrm{Pr}}$(MeCN)·$SbF_6$ may be influenced by the steric repulsion between the isopropyl methyl groups and the TACH skeleton. This repulsion may have induced the depression of the metal atom by other isopropyl methyl groups as described above. This small displacement makes the donating ability of the amines weaker and shifts the redox potential to a positive region. Additionally, the smaller ΔE_p value for $\mathbf{1}^{i\mathrm{Pr}}$(MeCN)·$SbF_6$ (99 mV) compared to those of $\mathbf{1}^{\mathrm{Et}}$(MeCN)·SbF_6 (109 mV), $\mathbf{1}^{i\mathrm{Bu}}$(MeCN)·$SbF_6$ (113 mV), and $\mathbf{1}^{\mathrm{Bn}}$(MeCN)·SbF_6 (105 mV) indicates that its electrochemical reversibility between the Cu$^{\mathrm{I}}$ and Cu$^{\mathrm{II}}$ states is smoother than those of the other complexes. This suggests that $\mathbf{1}^{i\mathrm{Pr}}$(MeCN)·$SbF_6$ has an efficient reversible oxygenation ability.

Reactions of Copper(I) Complexes with O_2

As expected from its electrochemical properties, $\mathbf{1}^{i\mathrm{Pr}}$(MeCN)·$SbF_6$ reacts with O_2 in THF or acetone at –80 °C, and the solution immediately changes from colorless to purple. The UV/Vis (Figure 5), resonance Raman, and ESR spectral features of the purple solution suggest the formation of $\mathbf{2}^{i\mathrm{Pr}}$ with a (μ-η²:η²-peroxido)dicopper(II) core.[6,7,9,21] This complex is ESR-silent, indicating that there is an antiferromagnetic interaction between the two copper(II) ions. The complex in solution has two characteristic absorption bands at 362 (ε = 20000) and 526 (ε = 1400) nm, which are assigned as $\pi_\sigma^* \rightarrow d_{xy}$ and $\pi_v^* \rightarrow d_{xy}$ charge-transfer bands originating from the peroxido oxygen atom to the copper(II) ion for the (μ-η²:η²-peroxido)dicopper(II) species. These absorption bands are very similar to those of the previously reported (μ-η²:η²-peroxido)dicopper(II) species[9] as well as those of oxyHc[46,47] and oxyTy.[8,48,49] This feature is clearly different from those of the bis(μ-oxido)-dicopper(III) ($\mathbf{3}^{\mathrm{R}}$) species generated from copper(I) complexes with Et$_3$TACH, *i*Bu$_3$TACH, and Bn$_3$TACH reported previously (Table 7).

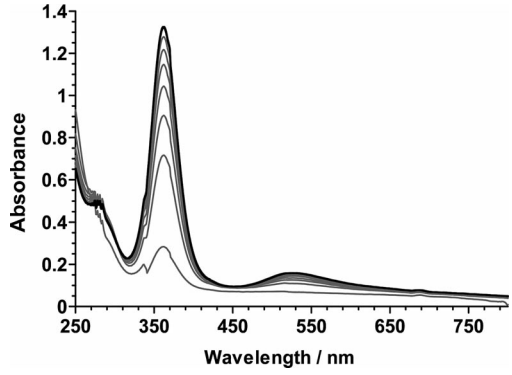

Figure 5. Electronic absorption spectral change developed on oxygenating $\mathbf{1}^{i\mathrm{Pr}}$(MeCN)·$SbF_6$ in THF at –80 °C (0.07 mM).

Tolman et al. previously reported that the copper complex system with *i*Pr$_3$TACN undergoes an interconversion between the (μ-η²:η²-peroxido)dicopper and bis(μ-oxido)dicopper species when different solvents are used. The former is generated in CH_2Cl_2, and the latter is generated in THF.[24,25] In our case, only the (μ-η²:η²-peroxido)dicopper species is formed at –80 °C in THF, CH_2Cl_2, and acetone and also at –120 °C in MeTHF (Figure S3), although it was observed that the complex is unstable in CH_2Cl_2 at –80 °C.

Table 7. UV/Vis and Raman spectroscopic data for $\mathbf{2}^{i\mathrm{Pr}}$ and $\mathbf{3}^{\mathrm{R}}$ (R = Et, *i*Bu, and Bn).

Complex	λ_{max} [nm] (ε [M^{-1} cm^{-1}])	ν(^{16}O–^{16}O) [ν(^{18}O–^{18}O)] [cm^{-1}]	ν(Cu–^{16}O) [ν(Cu–^{18}O)] [cm^{-1}]	Ref.
$\mathbf{2}^{i\mathrm{Pr}}$	362 (20000), 526 (1400)	757 [715]		this work
$\mathbf{3}^{\mathrm{Et}}$	309 (15000), 408 (18000)		553, 581 [547]	[43]
$\mathbf{3}^{i\mathrm{Bu}}$	321 (16000), 412 (19000)		571 [546]	[42]
$\mathbf{3}^{\mathrm{Bn}\text{-}d2}$	308 (17000), 413 820000)		585 [560]	[43]

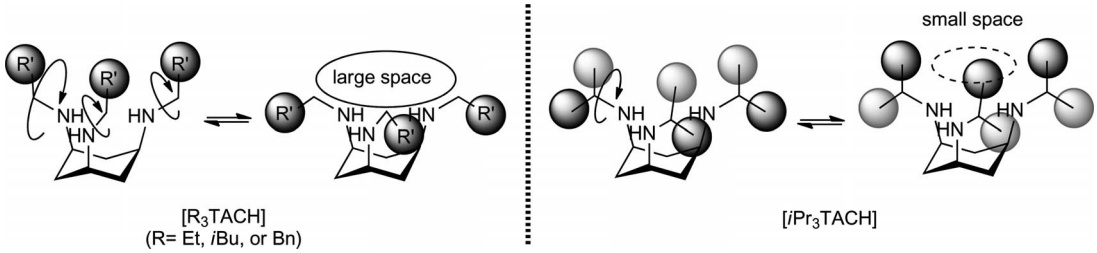

Figure 6. Rotations around the N–C bond in R_3TACH and iPr$_3$TACH.

Such an interconversion was not observed for this system in any organic solvent used here. This behavior may be a result of the ability of the ethyl, isobutyl, and benzyl groups of Et_3TACH, iBu$_3$TACH, and Bu_3TACH, respectively, to rotate around the N–C bond. The small –CH_2– groups in Et_3TACH, iBu$_3$TACH, and Bu_3TACH would allow free rotation unimpeded by intramolecular steric hindrance between two ligands in the side-on peroxido complex, although it is not impossible for the isopropyl group in iPr$_3$-TACH to rotate around the N–C bond (Figure 6).

The isopropyl group of iPr$_3$TACH may cause steric hindrance and disturb the rotation of the dimethyl groups of the isopropyl substituent. In the iPr$_3$TACH system, it may be difficult to form a dinuclear complex with a short Cu···Cu distance as is formed in the bis(μ-oxido)dicopper core in the copper systems with Et_3TACH, iBu$_3$TACH, and Bn_3TACH.

Evidence for the formation of the (μ-η^2:η^2-peroxido)dicopper species is indicated by resonance Raman spectral measurements of the reaction product of **2**$^{i\mathrm{Pr}}$ with $^{16}O_2$/$^{18}O_2$ dioxygen. A band at 757/715 cm^{-1} is visible, which is assignable to an O–O stretching vibration band of a peroxido species, ν(^{16}O–^{16}O)/ν(^{18}O–^{18}O) (Figure 7). This stretching vibration is similar to that of native oxyTy (755/714 cm^{-1}), although it has a slightly higher value than that of oxyHc (741/697 cm^{-1}). For the O–O stretching vibration bands of (μ-η^2:η^2-peroxido)dicopper(II) species of the model systems observed hitherto,[9,13,50,51] those of the (μ-η^2:η^2-peroxido)-dicopper(II) species coordinated with π-system ligands (725–765 cm^{-1}), such as imidazole, pyridine, or pyrazole, are observed in a comparatively higher energy region than complexes with σ-donating ligands (713–739 cm^{-1}), such as secondary and tertiary amines. However, all three of the coordinating atoms of the iPr$_3$TACH ligand are σ-donating amines. This may be explained as follows: the approach of two copper ions has been restricted by the steric repulsion between the isopropyl groups of iPr$_3$TACH ligands when the (μ-η^2:η^2-peroxido)dicopper(II) core is formed, so the O–O bond in this system cannot be further weakened because of its steric restriction.

We attempted to obtain **2**$^{i\mathrm{Pr}}$ as a solid, and, fortunately, a purple precipitate was obtained from a THF solution at –80 °C upon standing overnight. As the solubility of this precipitate in THF is low, a UV/Vis spectrum of the purple solid was measured by dissolving it in acetone. The spectrum is similar to that of the (μ-η^2:η^2-peroxido)dicopper complex **2**$^{i\mathrm{Pr}}$, indicating that **2**$^{i\mathrm{Pr}}$ is isolable as a solid. However, we have been unable to obtain a single crystal suitable for X-ray analysis. We tested **1**$^{i\mathrm{Pr}}$(MeCN)·SbF_6 for reversible oxygenation. The **1**$^{i\mathrm{Pr}}$ species reacts with dioxygen to generate an O_2 adduct under O_2 at –70 °C in acetone. This adduct releases O_2 at 0 °C with Ar bubbling. After three cycles of O_2 binding and release, the extent of decomposition of **2**$^{i\mathrm{Pr}}$ was about 10% as judged from the absorption intensity (Figure 8).

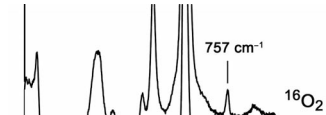

Figure 7. Resonance Raman spectra of a THF solution of **1**$^{i\mathrm{Pr}}$(MeCN)·SbF_6 treated with $^{16}O_2$ (upper line) and $^{18}O_2$ (bottom line) at –80 °C (λ_{ex} = 532 nm).

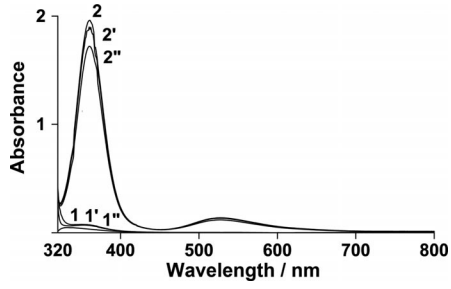

Figure 8. Electronic absorption spectra showing the reversible O_2 binding of **1**$^{i\mathrm{Pr}}$·SbF_6 in acetone. Spectrum 2 was obtained from the solution of **2**$^{i\mathrm{Pr}}$. Spectrum 1 was obtained after Ar bubbling at 0 °C. Spectrum 2′ was obtained after O_2 addition to the resultant solution. Spectra 1′, 2′′, and 1′′ were observed after the second and third cycles.

Decomposition of the (μ-η^2:η^2-Peroxido)dicopper Complex

We previously reported that the bis(μ-oxido)dicopper-(III) complex with Et_3TACH converts to the bis(μ-hydroxido)dicopper(II) complex in a reaction with THF.[42]

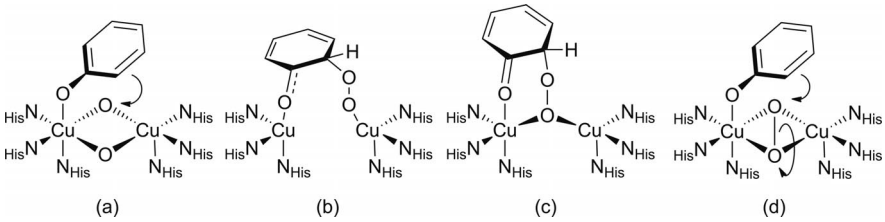

Figure 9. Possible mechanisms of phenol hydroxylation catalyzed by Ty.

However, the (μ-carbonato)dicopper(II) species, as measured using ESI-TOF-MS, was detected as a decomposition product of the (μ-η²:η²-peroxido)dicopper(II) complex with iPr$_3$TACH, **2**$^{i\mathrm{Pr}}$, and the bis(μ-hydroxido)dicopper(II) species, which was detected in the decomposition products of $[Cu_2(O)_2(Et_3TACH)_2]^{2+}$ reported previously, was not observed in this system. Additionally, the bis(μ-hydroxido)dicopper(II) species was not generated by the reaction of CuX_2 (X = Cl, OTf) with the iPr$_3$TACH ligand. This may mean that the (μ-η²:η²-peroxido)dicopper(II) complex with iPr$_3$TACH, **2**$^{i\mathrm{Pr}}$, does not generate the bis(μ-oxido)dicopper(III) species in the reaction.

It is notable that the Cu···Cu distance for the bis(μ-hydroxido)dicopper(II) complex with the Tp$^{i\mathrm{Pr},i\mathrm{Pr}}$ ligand is 2.937 Å.[52] This distance is shorter than those of the present type of (μ-η²:η²-peroxido)dicopper(II) complex (3.2–3.6 Å).[9] This suggests that it is difficult to form the dinuclear copper complex if the Cu···Cu distance is short. We previously reported that bis(μ-oxido)dicopper(III) complexes with R$_3$TACH (R = *i*Bu and Bn) decomposed with accompanying *N*-dealkylation.[43] Tolman et al. also reported that bis(μ-oxido)dicopper(III) complexes with iPr$_3$TACN decompose with *N*-dealkylation.[53] However, the decomposition products of **2**$^{i\mathrm{Pr}}$, which are produced upon treatment with NH_4OH, only include free ligand as observed by ^{1}H NMR spectroscopy (Figure S4). These results indicate that the (μ-η²:η²-peroxido)dicopper(II) species is generated by the reaction of **1**$^{i\mathrm{Pr}}$(MeCN)·SbF_6 with dioxygen, but the bis(μ-oxido)dicopper(III) species has not been formed.

Oxygenation Reactivity

The hydroxylation of phenol by the peroxido complex **2**$^{i\mathrm{Pr}}$ was investigated using the sodium salt of 2,4-di-*tert*-butylphenol as a phenol model in CH_2Cl_2 at –95 °C. The solution of **2**$^{i\mathrm{Pr}}$ immediately changed from purple to green upon addition of the phenolate salt. From the reaction products, the *ortho*-quinone was obtained in 50% yield based on the peroxido intermediate, but the C–C coupling dimer of phenol, which is occasionally obtained in such a reaction[54] was also produced. The oxidation reaction was carried out under N_2, so the quinone obtained in this reaction may have been generated by disproportionation of semiquinone[32] or oxygenation of phenolate by **2**$^{i\mathrm{Pr}}$. It is likely that such interactions involve coordination of phenolate to the metal atom. We failed to obtain any direct evidence of the binding of phenolate to the metal atom, although we also performed a stopped-flow spectroscopic measurement.

We previously reported that the bis(μ-oxido)dicopper(III) complexes of R$_3$TACH (R = Et, *i*Bu, and Bn) oxidize THF or have *N*-dealkylation of the TACH ligands. Phenolate was not oxidized. Interestingly, **2**$^{i\mathrm{Pr}}$ cannot oxidize THF and also has no *N*-dealkylation activity. We therefore conclude that **2**$^{i\mathrm{Pr}}$ oxidizes phenolate through coordination of the phenolate oxygen atom to the metal center in an electrophilic reaction. In the reaction of **2**$^{i\mathrm{Pr}}$ with phenolate, the conversion of (μ-η²:η²-peroxido)dicopper(II) to the bis(μ-oxido)dicopper species was not observed spectroscopically.

The reactivity of Ty towards phenolic substrates in nature has been previously reported and discussed, and various reaction mechanisms have been proposed.[33,35,37,40,55–58] For Ty, a number of peroxido O–O bond-cleavage mechanisms have been advanced. As shown in Figure 9,[57] (a) the binding of the phenolic oxygen atom to the metal ion initiates cleavage followed by attack of the aromatic ring, (b or c) the O–O bond cleavage occurs after the binding of dioxygen to the aromatic ring, and (d) O–O bond cleavage occurs concertedly in a reaction with the aromatic ring. In this study, we have succeeded in preparing only (μ-η²:η²-peroxido)dicopper species and in conversion of phenolate to *ortho*-quinone in a 50% yield based on the peroxido intermediate. We therefore propose the following hydroxylation mechanism for Ty activity: the cleavage of the peroxy O–O bond in Ty concertedly proceeds through the binding of phenolate to the copper ion.

Conclusions

We synthesized new copper(I) complexes with the iPr$_3$TACH ligand, which has tertiary α-carbon atoms, [Cu(MeCN)(iPr$_3$TACH)]X [**1**$^{i\mathrm{Pr}}$(MeCN)·X] (X = OTf, SbF_6) and [Cu(CO)(iPr$_3$TACH)]OTf [**1**$^{i\mathrm{Pr}}$(CO)·OTf]. Exposure of dioxygen to **1**$^{i\mathrm{Pr}}$(MeCN)·SbF_6 produces the corresponding (μ-η²:η²-peroxido)dicopper(II) species **2**$^{i\mathrm{Pr}}$ in THF or in acetone at –80 °C. This reactivity is quite different from the reactivity of the previously reported Cu$^{\mathrm{I}}$ complexes with other R$_3$TACH ligands, which have secondary α-carbon atoms (R = Et, *i*Bu, and Bn). These other complexes form bis(μ-oxido)dicopper(III) species in the reaction with dioxygen.[43] Resonance Raman spectra of the **2**$^{i\mathrm{Pr}}$ species have O–O stretching vibrations, $\nu(^{16}O–^{16}O)/\nu(^{18}O–^{18}O)$, at 757/715 cm^{-1}. This is a higher energy region than those of

the (μ-η²:η²-peroxido)dicopper(II) species, which have σ-donating amine ligands.[9] Species $\mathbf{2}^{i\mathrm{Pr}}$ is capable not only of reversible binding of dioxygen but also of hydroxylation of phenolate. This behavior is very similar to the reactivity of Hc, which exhibits Ty activity, although it is a dioxygen carrier protein. Complex $\mathbf{2}^{i\mathrm{Pr}}$ oxidizes phenolate to quinone, but does not react with THF. This is in contrast to the bis(μ-oxido)dicopper(III) complexes with R_3TACH (R = Et, *i*Bu, and Bn), which cannot oxidize phenolate but are capable of oxidizing THF or the *N*-dealkylation of the R_3TACH ligand.[43] This indicates that $\mathbf{2}^{i\mathrm{Pr}}$ oxidizes phenolate through coordination of the phenolate oxygen atom in the electrophilic reaction. Hydroxylation of phenolate proceeds only at the *ortho* position. We were unable to directly detect binding of phenolate by stopped-flow spectroscopy. We therefore propose that the hydroxylation mechanism of Ty includes cleavage of the peroxy O–O bond in Ty concertedly through the binding of phenolate to the copper ion. In this study, we succeeded in the selective preparation of (μ-η²:η²-peroxido)dicopper(II) and bis(μ-oxido)dicopper(III) species using copper(I) complexes with TACH derivative ligands. This success appears to be based on the specific structural features of the isopropyl group. When the copper(I) complex with $i\mathrm{Pr}_3$TACH reacts with dioxygen to form (μ-η²:η²-peroxido)dicopper(II), the repulsive van der Waals interaction between the opposing isopropyl groups improves the steric contact required for formation of the (μ-η²:η²-peroxido)dicopper(II) core. In Ty, such steric constraint may contribute to the formation of the (μ-η²:η²-peroxido)dicopper core.

Experimental Section

General: All reactions and manipulations of air-sensitive compounds were performed under dry Ar using conventional Schlenk techniques or in a glove box. Solvents were dried using standard methods and were freshly distilled under Ar before use (e.g. diethyl ether, toluene, and THF were purified by heating to reflux in the presence of sodium/benzophenone, and dichloromethane was heated to reflux in the presence of CaH_2). Dry sodium 2,4-di-*tert*-butylphenolate was prepared according to a reported procedure.[59] Electronic absorption spectra (UV/Vis spectra) were recorded with a JASCO V-570 spectrophotometer. IR spectra of the solid compounds were measured with a JASCO FT/IR-4200 spectrophotometer by the KBr disk method. Resonance Raman spectral measurements were carried out with an NKS-1000 spectrophotometer. X-band ESR spectra were obtained with a JEOL RE-1X spectrometer at 77 K. ^{1}H NMR spectral measurements were performed with a Bruker 600 MHz NMR spectrometer with $CDCl_3$ and CD_2Cl_2 solutions using Me_4Si as an internal standard. Elemental analyses were performed with a Perkin–Elmer Japan 2440II CHNO/S and corrected using acetanilide. Electrochemical measurements were performed in a glove box using a Bioanalytical Systems (BAS) ALS/CH Instruments Electrochemical Analyzer Model 600A, with a three-electrode system consisting of a glassy carbon working electrode, a Pt wire counter electrode, and an Ag/Ag^+ reference electrode. All measurements were carried out at room temperature with a sweep rate of 50 mV s^{-1} under Ar in a degassed CH_2Cl_2/MeCN (9:1, v/v) solution, using $n\mathrm{Bu}_4\mathrm{NClO}_4$ (TBAP) as a supporting electrolyte. The electrochemical potentials were corrected by measurement of the ferrocene/ferrocenium couple ($[Fe(C_5H_5)_2]/[Fe(C_5H_5)_2]^+$) ($E_{1/2}$ = 140 mV, ΔE = 104 mV). Electrospray ionization time-of-flight mass spectra (ESI-TOF-MS) were measured with a Micromass LCT spectrometer. Resonance Raman spectral measurements: Raman scattering was excited at 532.0 nm with an Ar laser (Laser Quantum, Ventus 532) and detected using a CCD detector (Andor, DU420-OE) attached to a single polychromator (Ritsu Oyo Kogaku, DG-1000). The slit width was set to 200 μm. The laser power used was 30 mW at the sample point. All measurements were carried out with samples contained in a spinning cell (3000 rpm) at room temperature. Raman shifts were calibrated with indene, and the accuracy of the peak positions of the Raman bands was ±1 cm^{-1}. X-ray crystallography: Single crystals of $\mathbf{1}^{i\mathrm{Pr}}$(MeCN)·$SbF_6$, $\mathbf{1}^{i\mathrm{Pr}}$(CO)·OTf, and $\mathbf{1}^{i\mathrm{Bu}}$(CO)·$PF_6$ suitable for X-ray diffrac-

Table 8. Crystallographic data and experimental details for $\mathbf{1}^{i\mathrm{Pr}}$(MeCN)·$SbF_6$, $\mathbf{1}^{i\mathrm{Pr}}$(CO)·OTf, and $\mathbf{1}^{i\mathrm{Bu}}$(CO)·$PF_6$.

	$\mathbf{1}^{i\mathrm{Pr}}$(MeCN)·$SbF_6$	$\mathbf{1}^{i\mathrm{Pr}}$(CO)·OTf	$\mathbf{1}^{i\mathrm{Bu}}$(CO)·$PF_6$
Empirical formula	$C_{17}H_{36}CuF_6N_4Sb$	$C_{17}H_{33}CuF_3N_3O_4S$	$C_{19}H_{39}CuF_6N_3OP$
Formula mass	595.78	496.07	534.05
Crystal system	orthorhombic	orthorhombic	monoclinic
Space group	$Pna2_1$ (No. 33)	$P2_12_12_1$ (No. 19)	$P2_1/n$ (No. 14)
a [Å]	18.338(14)	8.7036(3)	9.384(2)
b [Å]	7.990(6)	15.0294(8)	31.50(2)
c [Å]	16.072(12)	17.3872(11)	9.451(4)
β [°]	–	–	115.298(4)
V [Å^3]	2355(3)	2274.4(2)	2525(2)
Z	4	4	4
$\rho_{calcd.}$ [g cm^{-3}]	1.68	1.449	1.405
T [K]	173	173	173
μ(Mo-K_α) [cm^{-1}]	21.055	11.029	9.873
λ [Å]	0.71070	0.71070	0.71070
No. of reflections	16970	18132	22790
No. of unique reflections	5303	5203	7093
No. of observed reflections [$I > 3\sigma(I)$]	8051	12062	17390
No. of parameters	298	295	319
R_1 [$I > 3\sigma(I)$][a]	0.0580	0.0590	0.0561
wR_2 (all parameters)[b]	0.1257	0.1362	0.1853
GOF	0.882	1.033	0.991

[a] $R_1 = \Sigma||F_o| - |F_c||/\Sigma|F_o|$. [b] $wR_2 = \{\Sigma[w(F_o^2 - F_c^2)^2]/\Sigma w(F_o^2)_2\}^{1/2}$.

tion analyses were obtained from CH_2Cl_2/Et_2O or THF/Et_2O solutions upon standing for a few days under Ar. Each crystal was mounted on a glass fiber, and diffraction data were collected using a Rigaku/MSC Mercury CCD with graphite-monochromated Mo-K_α radiation at –100 °C. Crystal data and experimental details are listed in Table 8. All three structures were solved using a combination of direct methods (SIR 2004 and SIR 92) and Fourier techniques. All non-hydrogen atoms were refined anisotropically. Hydrogen atoms were refined using a riding model. A Sheldrick weighting scheme was applied. Plots of $\Sigma w(|F_o| - |F_c|)^2$ vs. $|F_o|$, reflection order in data collection, sin θ/λ, and various classes of indices showed no unusual trends. Neutral atomic scattering factors were taken from the International Tables for X-ray Crystallography.[60] Anomalous dispersion effects were included in F_c,[61] where the values for $\Delta f'$ and $\Delta f''$ were taken from those of Creagh and McAuley.[62] The values for the mass attenuation coefficients are those of Creagh and Hubbell.[63] All calculations were performed using the crystallographic software package CrystalStructure.[64,65] CCDC-870598 [for $\mathbf{1}^{i\mathrm{Pr}}$(MeCN)·$SbF_6$], -870597 [for $\mathbf{1}^{i\mathrm{Pr}}$(CO)·OTf], and -870596 [for $\mathbf{1}^{i\mathrm{Bu}}$(CO)·$PF_6$] contain the supplementary crystallographic data for this paper. These data can be obtained free of charge from The Cambridge Crystallographic Data Centre via www.ccdc.cam.ac.uk/data_request/cif.

***i*Pr₃TACH:** TACH·3HCl (2.02 g, 8.47×10^{-3} mol) and NaOH (1.02 g, 2.55×10^{-2} mol) were dissolved in water (10 mL) to give a clear solution. This was added to a solution of NaOAc (1.63 g) in acetic acid (9 mL), acetone (10 mL), and water (10 mL), which was cooled in an ice bath. Over 2 h, $NaBH_4$ (4.00 g, 1.06×10^{-1} mol) was added in small portions. After the addition was complete, the solution was warmed to room temperature and stirred for an additional 2 h. Sodium hydroxide [7% (w)] was added until a pH of 12 was reached, and then the aqueous phase was extracted with diethyl ether (40 mL × 4). The diethyl ether fractions were combined, washed once with a saturated salt solution (50 mL), and dried with $MgSO_4$. The solvent was evaporated to obtain a white solid (67.5%). $C_{15}H_{30}N_3{\cdot}2H_2O$ (219.47): calcd. C 61.81, H 12.79, N14.42; found C 61.61, H 12.82, N 14.25. FTIR (KBr): $\tilde{\nu}$ = 3268 (N–H), 2965, 2928 (aliphatic C–H), 1652 (N–H) cm^{-1}. ^1H NMR (600 MHz, $CDCl_3$): δ = 0.76 (q, 3 H, CH_{ax}), 1.04 [d, 18 H, $CH(CH_3)_2$], 1.28 (br., 3 H, NH), 2.16 (d, 3 H, CH_{eq}), 2.62 (tt, 3 H, CH), 3.00 [m, 3 H, $CH(CH_3)_2$] ppm. ESI-TOF-MS: m/z = 256.3 $[M + H]^+$.

Synthesis of Copper(I) Complexes: The preparations of copper(I) complexes were carried out under Ar in a glove box.

[Cu(MeCN)(*i*Pr₃TACH)]SbF₆ [$\mathbf{1}^{i\mathrm{Pr}}$(MeCN)·SbF₆]: iPr$_3$TACH (0.752 g, 2.94×10^{-3} mol) and [Cu(MeCN)$_4$](SbF$_6$) (1.382 g, 2.98×10^{-3} mol) were dissolved in THF (3 mL). The solution was stirred for 10 min. After adding Et_2O (5 mL), the solution was left standing for 10 h to obtain colorless crystals (1.48 g, 84.6%). $C_{17}H_{33}CuF_6N_4Sb$ (592.76): calcd. C 34.27, H 6.09, N 9.40; found C 33.78, H 6.24, N 9.22. FTIR (KBr): $\tilde{\nu}$ = 3288 (N–H), 2977, 2942 (aliphatic C–H), 2264 (C≡N), 658 (SbF_6) cm^{-1}. ^1H NMR (600 MHz, $CDCl_3$): δ = 0.77 (br., 3 H), 1.06 (s, 9 H), 1.21 (s, 9 H), 1.69 (br., 3 H), 2.04 (s, 3 H), 2.65 (br., 3 H), 2.98 (d, 3 H), 3.27 (s, 3 H) ppm. ESI-TOF-MS: m/z = 317.2 $[M - SbF_6]^+$.

[Cu(MeCN)(*i*Pr₃TACH)]OTf [$\mathbf{1}^{i\mathrm{Pr}}$(MeCN)·OTf]: This complex (yield 79.2%) was prepared according to the same method as [Cu(MeCN)(iPr$_3$TACH)]SbF$_6$ using [Cu(MeCN)$_4$](OTf) in place of [Cu(MeCN)$_4$](SbF$_6$). $C_{18}H_{36}CuF_3N_4O_3S$ (509.11): calcd. C 42.46, H 7.13, N 11.00; found C 42.40, H 7.20, N 10.85. FTIR (KBr): $\tilde{\nu}$ = 3257 (N–H), 2967, 2924 (aliphatic C–H), 2265 (C≡N), 1253 (as, SO_3), 1032 (sy, SO_3), 639 (C–S) cm^{-1}. ESI-TOF-MS: m/z = 317.2 $[M - OTf]^+$.

[Cu(CO)(*i*Pr₃TACH)]OTf [$\mathbf{1}^{i\mathrm{Pr}}$(CO)·OTf]: [Cu(MeCN)($iPr_3$TACH)](OTf) (89.2 mg, 1.75×10^{-4} mol) was dissolved in CH_2Cl_2 (3 mL), and the solution was stirred under CO (1 atm) at 0 °C for 1 h. The addition of Et_2O (5 mL) to the colorless solution yielded a white solid, which was subsequently recrystallized from CH_2Cl_2/Et_2O (66.6 mg, 76.5%). $C_{17}H_{34}CuF_3N_3O_4S$ (497.07): calcd. C 41.16, H 6.71, N 8.47; found C 41.08, H 6.78, N 8.34. FTIR (KBr): $\tilde{\nu}$ = 3282 (N–H), 2975, 2937 (aliphatic C–H), 2068 (C=O), 1260 (as, SO_3), 1032 (sy, SO_3), 638 (C–S) cm^{-1}. ESI-TOF-MS: m/z = 346.2 $[M - OTf]^+$.

[Cu(CO)(*i*Bu₃TACH)]PF₆ [$\mathbf{1}^{i\mathrm{Bu}}$(CO)·PF₆]: [Cu(CO)($iBu_3$TACH)]$PF_6$ was synthesized according to the previously reported method by using [Cu(MeCN)$_4$]PF_6 in place of [Cu(MeCN)$_4$]SbF_6 as a metal source.[43] Colorless crystals were obtained.

Ligand Recovery: $\mathbf{1}^{i\mathrm{Pr}}$(MeCN)·$SbF_6$ (60.0 mg, 1.01×10^{-5} mol) was dissolved in acetone (4 mL) under argon. Oxygen was bubbled through the solution at –70 °C, and the solution changed from colorless to purple. The mixture was stirred at –80 °C for 3 h and warmed to room temperature. After the addition of CH_2Cl_2 (15 mL), the mixture was washed with 5% NH_4OH (2 × 5 mL) and water (2 × 10 mL). The organic layer was dried with $MgSO_4$ and filtered, and volatile materials were removed in vacuo to leave a pale-yellow solid (20.5 mg). ^1H NMR (600 MHz, $CDCl_3$): 0.76 (q, 3 H, CH_{ax}), 1.04 [d, 18 H, $CH(CH_3)_2$], 2.16 (d, 3 H, CH_{eq}), 2.62 (tt, 3 H, CH), 3.00 [m, 3 H, $CH(CH_3)_2$] ppm.

Oxidation Reaction of Phenolate: A solution of $\mathbf{1}^{i\mathrm{Pr}}$(MeCN)·$SbF_6$ (11.8 mg, 2.0×10^{-5} mol) in CH_2Cl_2 (2 mL) was stirred under oxygen at –95 °C for 3 min. The solution changed from colorless to purple. After vacuum/pumping with N_2 gas several times, a solution of sodium 2,4-di-*tert*-butylphenolate (4.6 mg, 2.0×10^{-5} mol) in CH_2Cl_2 was added to the mixture, and the color immediately changed to green. The solution was stirred for 3 h and was then warmed to room temperature. The addition of *n*-hexane (10 mL) to the solution resulted in the precipitation of the Cu complexes. After filtration and addition of 1-chloronaphthalene as an internal standard, the reaction products were monitored by GC. For ^{18}O tracing experiments, the reactions were carried out using $^{18}O_2$, and incorporation of ^{18}O into quinone products was confirmed by EI-MS (Figure S5).

GC Conditions: Column DB-5 ms; column length 30.0 m; column temperature 100 °C (heating to 200 °C at a rate of 10 °C min^{-1} with an interval of 10 min); injection temperature 200 °C; 62.7 kPa. 1-Chlorobenzene was used as an internal standard. The retention time of 3,5-Di-*tert*-butylbenzoquinone is 19.8 min.[66]

Supporting Information (see footnote on the first page of this article): Filling models (views from the upper site) of cationic parts of $\mathbf{1}^{i\mathrm{Pr}}$(MeCN)·$SbF_6$, $\mathbf{1}^{\mathrm{Et}}$(MeCN)·SbF_6, $\mathbf{1}^{i\mathrm{Bu}}$(MeCN)·$SbF_6$, and $\mathbf{1}^{\mathrm{Bn}}$(MeCN)·SbF_6; cyclic voltammogram of $\mathbf{1}^{i\mathrm{Pr}}$(MeCN)·$SbF_6$; electronic absorption spectrum in MeTHF at –120 °C (0.1 mM); ^1H NMR spectrum in $CDCl_3$ of the extracted products after the reaction of $\mathbf{1}^{i\mathrm{Pr}}$(MeCN)·$SbF_6$ with dioxygen; GC and EI-MS data for products obtained from the reaction of $\mathbf{2}^{i\mathrm{Pr}}$ with sodium 2,4-di-*tert*-butylphenolate.

Acknowledgments

We gratefully acknowledge the support of this work by a Grant-in-Aid for Scientific Research from the Ministry of Education, Culture, Sports, Science, and the Knowledge Cluster Project.

[1] A. De, S. Mandal, R. Mukherjee, *J. Inorg. Biochem.* **2008**, *102*, 1170–1189.
[2] V. Mahadevan, R. K. Gebbink, T. D. P. Stack, *Curr. Opin. Chem. Biol.* **2000**, *4*, 228–234.
[3] E. I. Solomon, P. Chen, M. Metz, S.-K. Lee, A. E. Palmer, *Angew. Chem.* **2001**, *113*, 4702; *Angew. Chem. Int. Ed.* **2001**, *40*, 4570–4590.
[4] S. Schindler, *Eur. J. Inorg. Chem.* **2000**, 2311–2326.
[5] T. D. P. Stack, *Dalton Trans.* **2003**, 1881–1889.
[6] E. A. Lewis, W. B. Tolman, *Chem. Rev.* **2004**, *104*, 1047–1076.
[7] N. Kitajima, Y. Moro-oka, *Chem. Rev.* **1994**, *94*, 737–757.
[8] E. I. Solomon, U. M. Sundaram, T. E. Machonkin, *Chem. Rev.* **1996**, *96*, 2563–2605.
[9] L. M. Mirica, X. Ottenwaelder, T. D. P. Stack, *Chem. Rev.* **2004**, *104*, 1013–1045.
[10] W. B. Tolman, *Acc. Chem. Res.* **1997**, *30*, 227–237.
[11] L. Que Jr., W. B. Tolman, *Nature* **2008**, *455*, 333–340.
[12] K. E. van Holde, K. I. Miller, H. Decker, *J. Biol. Chem.* **2001**, *276*, 15563–15566.
[13] M. Rolff, J. Schottenheim, H. Decker, F. Tuczek, *Chem. Soc. Rev.* **2011**, *40*, 4077–4098.
[14] S. Itoh, S. Fukuzumi, *Acc. Chem. Res.* **2007**, *40*, 592–600.
[15] H. Decker, T. Schweikardt, F. Tuczek, *Angew. Chem.* **2006**, *118*, 4658; *Angew. Chem. Int. Ed.* **2006**, *45*, 4546–4550.
[16] C. Gerdemann, C. Eicken, B. Krebs, *Acc. Chem. Res.* **2002**, *35*, 183–191.
[17] M. E. Cuff, K. I. Miller, K. E. Van Holde, W. A. Hendrickson, *J. Mol. Biol.* **1998**, *278*, 855–870.
[18] E. J. Land, C. A. Ramsden, P. A. Riley, *Acc. Chem. Res.* **2003**, *36*, 300–308.
[19] C. M. Marusek, N. M. Trobaugh, W. H. Flurkey, J. K. Inlow, *J. Inorg. Biochem.* **2006**, *100*, 108–123.
[20] Y. Matoba, T. Kumagai, A. Yamamoto, H. Yoshitsu, M. Sugiyama, *J. Biol. Chem.* **2006**, *281*, 8981–8990.
[21] N. Kitajima, K. Fujisawa, Y. Moro-oka, K. Toriumi, *J. Am. Chem. Soc.* **1989**, *111*, 8975–8976.
[22] K. A. Magnus, B. Hazes, H. Ton-That, C. Bonaventura, J. Bonaventura, W. G. J. Ho, *Proteins: Struct., Funct., Genet.* **1994**, *19*, 302–309.
[23] K. A. Magnus, H. Ton-That, J. E. Carpenter, *Chem. Rev.* **1994**, *94*, 727–735.
[24] J. A. Halfen, S. Mahapatra, E. C. Wilkinson, S. Kaderli, V. G. Young Jr., L. Que Jr., A. D. Zuberbühler, W. B. Tolman, *Science* **1996**, *271*, 1397–1400.
[25] J. Cahoy, P. L. Holland, W. B. Tolman, *Inorg. Chem.* **1999**, *38*, 2161–2168.
[26] J. Lewin, D. Heppner, C. Cramer, *J. Biol. Inorg. Chem.* **2007**, *12*, 1221–1234.
[27] Y. Funahashi, T. Nishikawa, Y. Wasada-Tsutsui, Y. Kajita, S. Yamaguchi, H. Arii, T. Ozawa, K. Jitsukawa, T. Tosha, S. Hirota, T. Kitagawa, H. Masuda, *J. Am. Chem. Soc.* **2008**, *130*, 16444–16445.
[28] L. Casella, E. Monzani, M. Gullotti, D. Cavagnino, G. Cerina, L. Santagostini, R. Ugo, *Inorg. Chem.* **1996**, *35*, 7516–7525.
[29] E. Monzani, L. Quinti, A. Perotti, L. Casella, M. Gullotti, L. Randaccio, S. Geremia, G. Nardin, P. Faleschini, G. Tabbì, *Inorg. Chem.* **1998**, *37*, 553–562.
[30] L. Santagostini, M. Gullotti, E. Monzani, L. Casella, R. Dillinger, F. Tuczek, *Chem. Eur. J.* **2000**, *6*, 519–522.
[31] G. Battaini, M. De Carolis, E. Monzani, F. Tuczek, L. Casella, *Chem. Commun.* **2003**, *9*, 726–727.
[32] S. Palavicini, A. Granata, E. Monzani, L. Casella, *J. Am. Chem. Soc.* **2005**, *127*, 18031–18036.
[33] S. Itoh, H. Kumei, M. Taki, S. Nagatomo, T. Kitagawa, S. Fukuzumi, *J. Am. Chem. Soc.* **2001**, *123*, 6708–6709.
[34] T. Osako, K. Ohkubo, M. Taki, Y. Tachi, S. Fukuzumi, S. Itoh, *J. Am. Chem. Soc.* **2003**, *125*, 11027–11033.
[35] L. M. Mirica, M. Vance, D. J. Rudd, B. Hedman, K. O. Hodgson, E. I. Solomon, T. D. P. Stack, *Science* **2005**, *308*, 1890–1892.
[36] B. T. Op't Holt, M. A. Vance, L. M. Mirica, D. E. Heppner, T. D. P. Stack, E. I. Solomon, *J. Am. Chem. Soc.* **2009**, *131*, 6421–6438.
[37] A. Company, S. Palavicini, I. Garcia-Bosch, R. Mas-Ballest, L. Que Jr., E. V. Rybak-Akimova, L. Casella, X. Ribas, M. Costas, *Chem. Eur. J.* **2008**, *14*, 3535–3538.
[38] I. Garcia-Bosch, X. Ribas, M. Costas, *Chem. Eur. J.* **2012**, *18*, 2113–2122.
[39] I. Garcia-Bosch, A. Company, J. R. Frisch, M. Torrent-Sucarrat, M. Cardellach, I. Gamba, M. Güell, L. Casella, J. Lawrence Que, X. Ribas, J. M. Luis, M. Costas, *Angew. Chem.* **2010**, *122*, 2456; *Angew. Chem. Int. Ed.* **2010**, *49*, 2406–2409.
[40] A. Spada, S. Palavicini, E. Monzani, L. Bubacco, L. Casella, *Dalton Trans.* **2009**, 6468–6471.
[41] M. Rolff, J. Schottenheim, G. Peters, F. Tuczek, *Angew. Chem.* **2010**, *122*, 6583; *Angew. Chem. Int. Ed.* **2010**, *49*, 6438–6442.
[42] H. Arii, Y. Saito, S. Nagatomo, T. Kitagawa, Y. Funahashi, K. Jitsukawa, H. Masuda, *Chem. Lett.* **2003**, *32*, 156–157.
[43] Y. Kajita, H. Arii, T. Saito, Y. Saito, S. Nagatomo, T. Kitagawa, Y. Funahashi, T. Ozawa, H. Masuda, *Inorg. Chem.* **2007**, *46*, 3322–3335.
[44] B. M. T. Lam, J. A. Halfen, V. G. Young Jr., J. R. Hagadorn, P. L. Holland, A. Lledós, L. Cucurull-Sánchez, J. J. Novoa, S. Alvarez, W. B. Tolman, *Inorg. Chem.* **2000**, *39*, 4059–4072.
[45] L. C. Pauling, *The nature of the chemical bond and the structure of molecules and crystals: an introduction to modern structural chemistry*, 3rd ed., Cornell University Press, Ithaca, **1960**.
[46] K. Heirwegh, H. Borginon, R. Lontie, *Biochim. Biophys. Acta* **1961**, *48*, 517–526.
[47] K. E. Van Holde, *Biochemistry* **1967**, *6*, 93–99.
[48] K. Lerch, L. Ettinger, *Eur. J. Biochem.* **1972**, *31*, 427–437.
[49] M. Huber, K. Lerch, *Biochemistry* **1988**, *27*, 5610–5615.
[50] H.-C. Liang, M. J. Henson, L. Q. Hatcher, M. A. Vance, C. X. Zhang, D. Lahti, S. Kaderli, R. D. Sommer, A. L. Rheingold, A. D. Zuberbuhler, E. I. Solomon, K. D. Karlin, *Inorg. Chem.* **2004**, *43*, 4115–4117.
[51] L. Q. Hatcher, M. A. Vance, A. A. Narducci Sarjeant, E. I. Solomon, K. D. Karlin, *Inorg. Chem.* **2006**, *45*, 3004–3013.
[52] T. Beissel, B. S. P. C. D. Vedova, K. Wieghardt, R. BoeseIb, *Inorg. Chem.* **1990**, *29*, 1736–1741.
[53] S. Mahapatra, J. A. Halfen, E. C. Wilkinson, G. Pan, X. Wang, V. G. Young Jr., C. J. Cramer, L. Que Jr., W. B. Tolman, *J. Am. Chem. Soc.* **1996**, *118*, 11555–11574.
[54] S. Mahapatra, J. A. Halfen, E. C. Wilkinson, J. Lawrence Que, W. B. Tolman, *J. Am. Chem. Soc.* **1994**, *116*, 9785–9786.
[55] P. K. Ross, E. I. Solomon, *J. Am. Chem. Soc.* **1991**, *113*, 3246–3259.
[56] E. I. Solomon, F. Tuczek, D. E. Root, C. A. Brown, *Chem. Rev.* **1994**, *94*, 827–856.
[57] H. Decker, R. Dillinger, F. Tuczek, *Angew. Chem.* **2000**, *112*, 1656; *Angew. Chem. Int. Ed.* **2000**, *39*, 1591–1595.
[58] S. Itoh, S. Fukuzumi, *Bull. Chem. Soc. Jpn.* **2002**, *75*, 2081–2095.
[59] S. Mandai, D. Macikenas, J. D. Protasiewicz, L. M. Sayre, *J. Org. Chem.* **2000**, *65*, 4804–4809.
[60] D. T. Cromer, J. T. Waber, *International Tables for X-ray Crystallography*, **1974**.
[61] J. A. Ibers, W. C. Hamilton, *Acta Crystallogr.* **1964**, *17*, 781–782.
[62] D. C. Creagh, W. J. McAuley, *International Tables for Crystallography*, **1992**, 219–222.
[63] D. C. Creagh, J. H. Hubbell, *International Tables for Crystallography*, **1992**, 200–206.
[64] *CrystalStructure 3, Crystal Structure Analysis Package*, Rigaku Corporation, Tokyo, **2000**.

[65] D. J. Watkin, C. K. Prout, J. R. Carruthers, P. W. Betteridge, *CRYSTALS Issue 10*, Chemical Crystallography Laboratory, University of Oxford, Oxford, **1996**.

[66] L. Q. Hatcher, K. D. Karlin, *J. Biol. Chem.* **2004**, *9*, 669–683.

Received: March 12, 2012
Published Online: ■

Dicopper Complexes

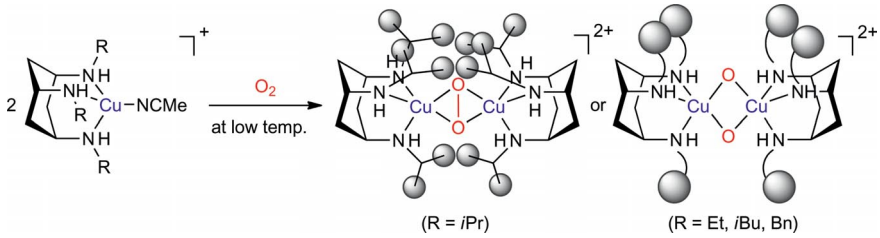

The selective preparation of (μ-η^2:η^2-peroxido)dicopper(II) and bis(μ-oxido)dicopper(III) species is regulated by the substituent groups of triaminocyclohexane derivative ligands. Their structural and spectroscopic features and reactivity are discussed.

J. Matsumoto, Y. Kajita, H. Masuda* 1–12

Synthesis and Characterization of a (μ-η^2:η^2-Peroxido)dicopper(II) Complex with *N,N′,N″*-Triisopropyl-*cis,cis*-1,3,5-triaminocyclohexane (R_3TACH, R = *i*Pr): Selective Preparation of (μ-η^2:η^2-Peroxido)dicopper(II) and Bis(μ-oxido)dicopper(III) Species Regulated by Substituent Groups

Keywords: Bioinorganic chemistry / Copper / Coordination modes / Hydroxylation

